Fructose-2,6-bisphosphate restores TDP-43 pathology-driven genome repair deficiency in motor neuron diseases

Anirban Chakraborty[a#], Joy Mitra[b#], Vikas H. Maloji Rao[b], Manohar Kodavati[b], Santi M. Mandal[d], Satkarjeet K. Gill[e], Sravan Gopalkrishnashetty Sreenivasmurthy[e], Velmarini Vasquez[b], Mikita Mankevich[d], Balaji Krishnan[e], Gourisankar Ghosh[d], Muralidhar L. Hegde[b,c,*], Tapas Hazra[a,*].

[a]Department of Internal Medicine, University of Texas Medical Branch, Galveston, TX, 77555, USA
[b]Division of DNA Repair Research, Center for Neuroregeneration, Department of Neurosurgery, Houston Methodist Research Institute, Houston, TX 77030, USA
[c]Department of Neuroscience, Weill Cornell Medical College, New York, NY 10065, USA
[d]Department of Chemistry and Biochemistry, University of California San Diego, LA Jolla, California 92093, USA
[e]Department of Neurology, Mitchell Center for Neurodegenerative Diseases, University of Texas Medical Branch, Galveston, TX 77555, USA

[#]Contributed equally

*Address of corresponding authors:

Muralidhar L Hegde, PhD
Professor, Center for Neuroregeneration
Department of Neurosurgery
Houston Methodist Research Institute, Houston, Texas 77030, USA
Tel: (713) 441-7456
E-mail: mlhegde@houstonmethodist.org

Tapas Hazra, PhD
Professor, Department of Internal Medicine-Pulmonary, Critical Care & Sleep Medicine
University of Texas Medical Branch, Galveston, TX 77555, USA
Tel: (409) 772-6308
Fax: (409) 747-8608
E-mail: tkhazra@utmb.edu

Abstract
TAR DNA-binding protein 43 (TDP-43) proteinopathy plays a critical role in neurodegenerative diseases, including amyotrophic lateral sclerosis and frontotemporal dementia (FTD). In our recent discovery, we identified that TDP-43 plays an essential role in DNA double-strand break (DSB) repair via the non-homologous end joining (NHEJ) pathway. Here, we found persistent DNA damage in the brains of ALS/FTD patients, primarily in the transcribed regions of the genome. We further investigated the underlying mechanism and found that polynucleotide kinase 3'-phosphatase (PNKP) activity was severely impaired in the nuclear extracts of both patient brains and TDP-43-depleted cells. PNKP is a key player in DSB repair within the transcribed genome, where its 3'-P termini processing activity is crucial for preventing persistent DNA damage and neuronal death. The inactivation of PNKP in ALS/FTD was due to reduced levels of its interacting partner, phosphofructo-2-kinase fructose 2,6 bisphosphatase (PFKFB3), and its biosynthetic product, fructose-2,6-bisphosphate (F2,6BP), an allosteric modulator of glycolysis. Recent work from our group has shown that F2,6BP acts as a positive modulator of PNKP activity *in vivo*. Notably, exogenous supplementation with F2,6BP restored PNKP activity in nuclear extracts from ALS/FTD brain samples and patient-derived induced pluripotent stem (iPS) cells harboring pathological mutations. Furthermore, we demonstrate that supplementation of F2,6BP restores genome integrity and partially rescues motor phenotype in a *Drosophila* model of ALS. Our findings underscore the possibility of exploring the therapeutic potential of F2,6BP or its analogs in TDP-43 pathology-associated motor neuron diseases.

Keywords: TDP-43, PNKP, DNA damage, amyotrophic lateral sclerosis, PFKFB3.

Introduction

Amyotrophic lateral sclerosis and frontotemporal dementia (FTD) are neurodegenerative diseases marked by dysfunction and toxicity of TAR DNA-binding protein 43 (TDP-43), which drives progressive neuronal degeneration (1-5). TDP-43 pathology in these diseases is characterized by the loss of nuclear TDP-43 and its accumulation in the cytoplasm, disrupting cellular pathways in motor neurons (6, 7). Our recent studies demonstrated that TDP-43 plays a key role in the classical non-homologous end-joining (C-NHEJ) pathway, which is primarily responsible for repairing DNA double-strand breaks (DSBs) in neurons. Upon DNA damage, TDP-43 is rapidly recruited at DSB sites, where it stably interacts with DNA damage response (DDR) and NHEJ factors, facilitating the recruitment of break-sealing XRCC4-Lig4 complex in induced pluripotent stem cell (iPSC)-derived motor neurons (5, 8-12). We found that mislocalization of ALS-associated mutant TDP-43 significantly impairs NHEJ-mediated DNA repair, leading to the accumulation of DNA damage, cellular senescence, and increased neuroinflammation (13). Notably, the compromised NHEJ repair in TDP-43 proteinopathy is associated with reduced recruitment of XRCC4/Lig4 at DSB sites (5, 10), though the precise mechanism by which TDP-43 regulates C-NHEJ remains unclear.

In ALS and FTD cases, enhanced production of reactive oxygen species (ROS) and persistent inflammation can lead to oxidative genome damage and DNA single-strand (SSB) and double-strand breaks (DSBs) (14-18). Polynucleotide kinase 3'-phosphatase (PNKP) is a bifunctional DNA end-processing enzyme with 3'-phosphatase and 5'-kinase activities (19, 20), and is a major 3'-phosphatase that is involved in both DNA BER/SSB and C-NHEJ-mediated DSB repair pathways in mammalian cells (21-24). Importantly, functional loss of PNKP in neuronal cells has been linked to several neuropathological conditions (25-30). Additionally, we have

shown that PNKP plays a critical role in the preferential repair of actively transcribed genomes via TC-SSBR and TC-NHEJ pathways, respectively (11, 12, 31-33). The 3´-phosphatase activity of PNKP is severely compromised in the two most prevalent polyQ neurodegenerative diseases, Huntington's disease (HD) (34) and spinocerebellar ataxia type 3 (SCA3) (32, 35).

Several studies provide strong mechanistic evidence linking metabolic reprogramming and DNA repair activity through the direct involvement of metabolic enzymes and metabolites, regulation of the dNTP pool, and metabolic regulation of epigenetic remodeling (36). The homodimeric 6-phosphofructo-2-kinase/fructose-2,6-bisphosphatases (PFKFBs) are the key glycolytic enzymes, which mediate the rate-limiting step in the process (37). Recently, PFKFB3 has been found to be translocated to the nucleus (38). The role of PFKFB3 in DSB repair via the HR pathway also has been demonstrated (39). To further investigate the molecular basis of PNKP inactivation in HD and SCA3, we observed that PNKP interacts with PFKFB3 and elucidated PFKFB3's role in TC-NHEJ. Notably, the levels of both PFKFB3 and its product, fructose-2,6 bisphosphate (F2,6BP), an allosteric modulator of glycolysis, are significantly lower in the nuclear extracts of post-mortem HD and SCA3 patient brains. Supplementation of F2,6BP in HD mouse striatal neuronal cells and HD flies fully restored nuclear and mitochondrial genome integrity and functionality (35, 40), suggesting F2,6BP to be a positive regulator of PNKP activity in vivo. Reduced level of PFKFB3 is therefore linked to decreased PNKP activity in HD and SCA3, connecting metabolic processes to DNA repair (32, 35).

Since TDP-43, PNKP, and PFKFB3 are involved in NHEJ-mediated DSB repair, we investigated the role of PNKP and PFKFB3 in ALS and FTD models of TDP-43 pathology. We indeed observed a near-complete loss of 3'-phosphatase activity of PNKP, but not the protein level, in TDP-43-associated neurodegenerative conditions, correlating with TDP-43 mislocalization and persistent DNA damage. Notably, reduced PFKFB3 and F2,6BP levels have been observed in ALS/FTD patient tissues, indicating potential disruptions in glycolytic pathways that may exacerbate genomic instability associated with TDP-43 pathology. Importantly, such PNKP-mediated repair deficiency could be restored by exogenous supplementation of F2,6BP in extracts from ALS/FTD patient brains and patient-derived iPSCs. Notably, supplementation of F2,6BP partially rescued motor deficiency in a *Drosophila* model of ALS expressing human TDP-43 Q331K. Overall, our findings highlight the therapeutic potential of F2,6BP or its analogs in ALS/FTD and other neurodegenerative diseases associated with TDP-43 pathology.

Methods

Cell culture and Stable Line Generation

Human embryonic kidney HEK293 (ATCC) cells were cultured in Dulbecco's modified Eagle's medium (DMEM) with high glucose, supplemented with 10% fetal bovine serum (FBS) and 100 U/ml penicillin-streptomycin in a humidified chamber at 37°C and 5% CO_2.

To generate the PNKP-FLAG-expressing stable HEK293 cell line, coding DNA sequence of human PNKP (GenBank BC033822.1) was re-cloned to pFLAG-cDNA (Invitrogen/Life Technologies) between Pcmv and FLAG-tag encoding sequences within HindIII and BamHI sites. The gene in the newly constructed plasmid carried the natural Kozak sequence and nucleotides 97–1,669 of PNKP cDNA. The region containing Kozak-PNKP-FLAG was then transferred to pcDNA3.1-Hygro (Invitrogen/Life Technologies) within the HindIII-XbaI unique vector sites to generate the final plasmid, which was then used for creating a stable cell line

resistant to hygromycin (Hygro), following standard procedures (21). Ectopic expression of PNKP was confirmed by western blotting of whole-cell extract using anti-FLAG Ab (Sigma, F1804).

siRNA transfection

TDP-43 depletion was carried out in HEK293 cells using siRNAs (80 nM; transfected twice on consecutive days) against the *TARDBP* gene. The cells were transfected with control siRNA (siControl) or TDP-43-specific siRNA (siTDP-43; Thermo Fisher; Silencer Select; 4392420) using lipofectamine 3000 (Invitrogen) for 6 h in optiMEM (Gibco; reduced serum media, 11058021), followed by replacing the medium with DMEM-High Glucose complete medium. Nuclear extracts were prepared from the harvested cells (72-96 h post-transfection) to examine the depletion of individual proteins by immunoblot (IB) analysis using specific antibodies. Lamin-B was used as the nuclear loading control.

Neural Progenitor Stem Cell (NPSC) Induction

Control and TDP-43 mutant induced pluripotent stem cells (iPSCs) were cultured on basement membrane matrix Geltrex LDEV-Free-coated Petri dishes using 1X Essential 8 media (Gibco, A1517001) and maintained in a humidified incubator at 37°C in 5% CO_2. To derive NPSCs, PSC neural induction media (Gibco A1647801) was used as per the manufacturer's protocol. The process involved replacing the Essential 8 media with PSC neural induction media approximately 24 h after sub-platting those iPSCs. This media was maintained for 7 days. The first passage (P0) NPSCs were then transferred onto Geltrex (Gibco, A1413201) coated 6-well plates and cultured in StemPRO neural stem cell SFM media (Gibco, A1050901). Neural induction efficiency was assessed at the third passage by immunofluorescence (IF) staining.
ALS-related TDP-43 G287S mutant and its CRISPR/Cas9-corrected isogenic TDP-43 S287G as well as FTD-related TDP-43 A382T along with C9ORF72 repeat mutation carrying iPSCs were kindly gifted by our collaborators Drs. Van Damme and Van Den Bosch (University of Leuven, Belgium). These lines were cultured according to their published protocol (41). Control and ALS patient-derived TDP-43 G298S mutant iPSC (NINDS, NH50216) lines were purchased from NIH-NINDS (42). Engineered homozygous TDP-43 Q331K mutant (Jax, JIPSC1064) and its isogenic control (Jax, JIPSC1104) lines were purchased from Jax iPSC.

Motor Neuron Differentiation

Motor neurons were generated from patient and control subject-derived iPSCs (NIH-NINDS & VIB-KU Leuven). The differentiation process followed established protocols with some modifications (43, 44). In brief, iPSC clones were transferred from a 60-cm dish to a T-25 flask filled with neuronal basic medium. The medium consisted of a mixture of 50% Neurobasal medium (Gibco, 21103049) and 50% DMEM/F12 medium (Gibco, 21331020), supplemented with N2 and B27 supplements without vitamin A. Collagenase type IV digestion was performed to facilitate suspension of the iPSC clones. Afterward, the suspended cell spheres were subjected to a series of incubations. Initially, they were treated with various inhibitors including 5 μM ROCK Inhibitor (Y-27632), 40 μM TGF-β inhibitor (SB 431524), 0.2 μM bone morphogenetic protein inhibitor (LDN-193189), and 3 μM GSK-3 inhibitor (CHIR99021). This was followed by incubation in a neuronal basic medium containing 0.1 μM retinoic acid (RA) and 500 nM Smoothened Agonist (SAG) for 4 days. Subsequently, the cell spheres were incubated for 2 days in a neuronal basic medium containing RA, SAG, 10 ng/ml Brain-derived neurotrophic factor

(BDNF), and 10 ng/ml Glial cell-derived neurotrophic factor (GDNF). To dissociate the cell spheres into single cells, they were exposed to a neuronal basic medium containing trypsin (0.025%)/DNase in a water bath at 37°C for 20 min. Afterward, the cells were pipetted into a medium containing trypsin inhibitor (1.2 mg/ml) to maintain their viability. Following cell counting, a specific number of cells were seeded onto dishes or chamber slides coated with 20 μg/ml Laminin. These cells were incubated for 5 days in a neuronal basic medium containing RA, SAG, BDNF, GDNF, and 10 μM DAPT. Subsequently, the medium was switched to one containing BDNF, GDNF, and 20 μM Inhibitor of γ-secretase (DAPT) for an additional 2 days. For motor neuron maturation, the cells were cultured in a medium containing BDNF, GDNF, and 10ng/ml ciliary neurotrophic factor (CNTF) for a period exceeding 7 days.

Immunoblotting (IB)

For IB analysis, cell lysates were extracted with 1x RIPA buffer (Millipore, 20-188) containing the protease inhibitor cocktail (Roche, 11836170001). Protein concentration was measured using 1x Bradford reagent (Biorad) in NanoDrop instrument. Then 20 μg protein per sample was loaded into NuPAGE 4–12% Bis-Tris precast (Invitrogen) gels for electrophoresis. After transfer to nitrocellulose membranes, the separated proteins were incubated with target primary and respective secondary antibodies, and the protein signals were detected by adding chemiluminescence reagents (LI-COR) and visualized by LI-COR Odyssey imaging system. HDAC2 and Lamin-B were used as loading controls as appropriate.

Co-immunoprecipitation (Co-IP)

Approximately 30 mg of brain tissues from ALS/FTD post-mortem patients or healthy controls (or ALS vs Sham mice brain cortices) were homogenized with 4 volumes of ice-cold homogenization buffer [0.25 M sucrose, 15 mM Tris-HCl, pH 7.9, 60 mM KCl, 15 mM NaCl, 5 mM EDTA, 1 mM EGTA, 0.15 mM spermine, 0.5 mM spermidine, 1 mM dithiothreitol (DTT), 0.1 mM phenylmethylsulfonyl fluoride (PMSF), and protease inhibitors (EDTA-free; Roche)]. Following homogenization, the homogenate was incubated on ice for 15 min and centrifuged at 1,000×g to obtain the cell pellet. Cells were lysed in Buffer A [10 mM Tris-HCl (pH 7.9), 0.34 M sucrose, 3 mM $CaCl_2$, 2 mM magnesium acetate, 0.1 mM EDTA, 1 mM DTT, 0.5% Nonidet P-40 (NP-40) and 1x protease inhibitor cocktail (Roche)] and centrifuged at 3,500×g for 15 min. Nuclear pellets were washed with Buffer A without NP-40 and then lysed in Buffer B [20 mM HEPES (pH 7.9), 3 mM EDTA, 10% glycerol, 150 mM potassium acetate, 1.5 mM $MgCl_2$, 1 mM DTT, 0.1% NP-40, 1 mM sodium orthovanadate (vanadate) and 1x protease inhibitors] by homogenization. Supernatants were collected after centrifugation at 15,000×g for 30 min and DNA/RNA in the suspension was digested with 0.15 U/μl benzonase (Novagen, 70-746-3) at 37°C for 1 h. The samples were centrifuged at 20,000×g for 30 min, and the supernatants collected as NEs. Co-IP was performed using anti-PNKP (BioBharati Life Science, BB-AB0105) antibody with Protein A/G PLUS agarose beads (Santa Cruz Biotechnology, sc2003) overnight, followed by four washes with Wash buffer [20 mM HEPES (pH 7.9), 150 mM KCl, 0.5 mM EDTA, 10% glycerol, 0.25% Triton-X-100 and 1x protease inhibitors] and eluted with Laemmli Sample Buffer (Bio-Rad; final concentration 1x). The immunoprecipitates were tested for the interacting proteins using appropriate Abs [PFKFB3 (GeneTexGTX108335), Lig 4 (GeneTex, GTX108820), RNAP II (Biolegend, 920202, pSer2, H5 Ab), and TDP-43 (Protein tech, 10782-2-AP).

3´-phosphatase activity assay of PNKP

The PNKP 3´-phosphatase activity in 1 µg of nuclear extracts (NE) of post-mortem ALS/FTD and age-matched patients' cortical tissues or with purified recombinant PNKP (2 ng) was conducted, as described previously (35). Five pmol of the radiolabeled substrate was incubated at 37°C for 15 min in buffer A (25 mM Tris-HCl, pH 8.0, 100 mM NaCl, 5 mM $MgCl_2$, 1 mM DTT, 10% glycerol and 0.1 µg/µl acetylated BSA). Five pmol of non-radiolabeled substrate was used as cold substrate. For in vitro PNKP restoration/abrogation, similar assays were done after incubation of F2,6BP/F6P/F1,6BP with the nuclear extracts for 15 min. The radioactive bands were visualized in PhosphorImager (GE Healthcare) and quantitated using ImageQuant software.

Enzymatic preparation of F2,6BP

Enzymatic preparations of F2,6BP were conducted, as we described earlier (35).

Estimation of F2,6BP in patient brain nuclear extracts

To quantify F2,6BP, the F6P assay kit (Sigma-Aldrich) was used to measure the amount of F6P before and after treating the crude nuclear extracts with 0.1M HCl and incubated at 37°C for 30 mins. Acid treatment converts F2,6BP into F6P. The assay was performed using the manufacturer's protocol which uses NADH-linked luciferase bioluminescence (35).

Long amplicon quantitative PCR (LA-qPCR)

Genomic DNA was extracted from cultured cells, autopsied brain tissues or adult *Drosophila* using the Genomic tip 20/G kit (Qiagen) per the manufacturer's protocol, to ensure minimal DNA oxidation during the isolation steps. The DNA was quantitated by Pico Green (Molecular Probes) in a black-bottomed 96-well plate and gene-specific LA qPCR assays were performed as described earlier (35) using Long Amp Taq DNA Polymerase (New England Biolabs). POLB and RNAPII (12.1 and 11.3 kb) were amplified from the experimental and control samples using appropriate oligos. Enolase/NeuroD (transcribed genes) and MyH2/MyH4 (non-transcribed genes) were amplified from human post-mortem samples. The list of primers used in this study is detailed in *Supplementary* **Table S2**.

The LA-qPCR reaction was set for all genes from the same stock of diluted genomic DNA (10-15 ng) sample, to avoid variations in PCR amplification during sample preparation. The final PCR reaction conditions were optimized at 94°C for 30 s; (94°C for 30 s, 55-60°C for 30 s depending on the oligo annealing temperature, 65°C for 10 min) for 25 cycles; 65°C for 10 min. Since amplification of a small region is independent of DNA damage, a small DNA fragment (~200-400 bp) from the corresponding gene(s) was also amplified for normalization of amplification of the large fragment. The amplified products were then visualized on gels and quantitated with ImageJ software (NIH).

Immunofluorescence (IF)

For NPSCs and motor neurons, the chamber slides were pre-coated with Geltrex and Matrigel, respectively, to facilitate cell adherence. Fixation of the cells for IF analysis was performed by replacing the media with a 1:1 ratio mixture of fresh media and 8% paraformaldehyde (PFA) in PBS, resulting in a final concentration of 4% PFA. Post-fixation, the slides were permeabilized using 0.2% Triton X-100 in 1x PBS, followed by blocking with 5% goat serum-TBS-T (1x TBS with 0.1% Tween-20) to prevent non-specific antibody binding. The cells were then incubated overnight at 4°C with target primary antibodies. Following this step, Alexa Fluor-488 (green) and

647-conjugated secondary antibodies (Thermo Fisher) were incubated for 1 h, and slides were then mounted with coverslips after applying DAPI-containing mounting media (Sigma-Aldrich, USA) to visualize the nuclei. Imaging was performed using a Zeiss Axio Observer 7 microscope or an Olympus Flouview3000 confocal microscope.

Proximity ligation assay (PLA)

PLA was conducted to investigate direct protein-protein interactions within cells. Approximately 20,000 cells were seeded per well in 8-well chamber slides for this experiment. After staining, cells underwent a washing step and were then fixed with 4% PFA for 15 min at room temperature. Subsequent steps included permeabilization in 0.2% Triton X-100 in 1x PBS for 10 min at RT, followed by PBS washing to remove any residual permeabilization agent. The in-situ PLA experiment was performed per the manufacturer's guidelines, using the DuoLink kit (Sigma-Aldrich, USA). After the PLA procedure, coverslips were mounted using DAPI mounting media (Sigma-Aldrich, USA), and imaging was performed using either a Zeiss Axio Observer 7 microscope or an Olympus Flouview3000 confocal microscope.

Immunohistochemistry (IHC)

Tissue samples were paraffin-embedded and sliced into 5 µm horizontal sections and mounted on glass slides. Slides were dewaxed and autoclaved for 10 min at 121°C in 0.01 M citrate buffer pH 6.0 for antigen retrieval. Immunostaining was performed using overnight incubation at 4°C with mouse anti-TDP-43 (R&D Systems, MAB77781, 1:200), and rabbit anti-phospho-TDP-43 (S409/410) (Proteintech, 80007-1-RR, 1:300). Nuclei were counterstained with DAPI. Slides were imaged on the next day in a confocal microscope.

Comet assay

The neutral comet assay was performed using the Comet Assay Kit (Trevigen, #4250-50-K), according to the manufacturer’s protocol to assess the extent of DNA DSBs in each sample. Briefly, singlet cell suspension was prepared by trypsinization of respective cell types in DPBS buffer, and about 200 cells were smeared in LM Agarose at 37°C in duplicate in each slide. The comet tails were visualized by staining the DNA with SYBR Green gold stain under a fluorescence microscope.

Drosophila Maintenance and Treatment

All Drosophila stocks were maintained at 25°C on standard fly food under a 12:12-h light–dark cycle. Drosophila strains were purchased from Bloomington Drosophila Stock Center (BDSC, Bloomington, Indiana, USA: UAS-TDP43 Q331K (RRID: BDSC_79590), expresses human TDP43 with ALS-linked mutation Q331K. The driver-P{GawB}OK6 (RRID: BDSC_64199) expresses GAL4 primarily in motor neurons. BDSC 79590 were crossed to BDSC_64199 and flies eclosed from the crosses were collected in fresh food vials and kept under standard conditions for 1 to 2 d for acclimatization. Flies were separated into two vials for Mock buffer and F2,6BP treatment. One BD syringe (1 mL) was filled with Mock buffer, and the other was filled with F2,6BP (50 µM) and drop is administered per day to respective cohorts at the same time of the day for 21 consecutive days.

Climbing or Negative Geotaxis Assay

The climbing assay was performed as described with minor modifications. Briefly, experimental flies were anesthetized on ice. A group of 10 flies (male and female mixed) per vial were transferred to a 25 mL sterile glass measuring cylinder. The measuring cylinder was divided into six compartments equally, the lowest compartment was labeled with 1 and the highest compartment was labeled with 6. The measuring cylinder with flies was placed against a white background for better video recording. The cylinder was tapped gently three times to send the flies to the bottom of the cylinder. The climbing time was recorded for 20 s. Five trials were performed for each cohort. The climbing score was calculated at 8 s.

Statistical analysis

All data are expressed as mean ± standard deviation (SD). Comparisons among experimental groups were carried out using Student's t-test, one-way or two-way ANOVA, as appropriate, for significance. Statistical analyses were performed using GraphPad Prism version 10 software. A p-value of less than 0.05 was considered statistically significant.

Results and Discussion

PNKP Activity is Significantly Reduced in ALS and FTD Patient Tissues

While our recent studies demonstrate the accumulation of DNA DSBs and a deficiency in NHEJ-mediated DSB repair in ALS patient brains with TDP-43 pathology (5), the potential link between PNKP and TDP-43 has not been investigated in the context of DNA DSB repair. Therefore, we assessed the impact of TDP-43 pathology on PNKP's 3'-phosphatase activity under ALS and FTD conditions (*Supplementary* **Figure S1A**) using a duplex oligo-based *in vitro* assay as schematically shown in **Figure 1A**. We observed a significant inhibition of PNKP activity in nuclear extracts (NE) from ALS-TDP-43 (Lns 5-7) and FTD-TDP-43 (Lns 8-9) cortical tissues, compared to age-matched non-neurological controls (Lns 2-4) (**Figure 1B**). We further validated this observation by exploiting a second cohort of Guamanian-ALS patients (Lns 6-9) and age-matched non-neurological control (Lns 2-5) brain cortical tissues and found a significant and comparable reduction in fold change of PNKP activity between the Guamanian-ALS and sporadic ALS cohorts, reinforcing the association between TDP-43 pathology and impaired PNKP function (**Figure 1C**). Demographic descriptions of ALS, FTD patients and age-matched non-neurological controls are detailed in *Supplementary* **Table S1**. Furthermore, we quantified relative PNKP levels in the analyzed patient specimens by immunoblotting (IB), which was largely unaffected compared to non-neurological controls (**Figure 1D**; *Supplementary* **Figure S1B**), indicating the loss of PNKP activity independent of its protein levels in ALS and FTD brains. These results collectively support the notion that PNKP dysfunction is prevalent in ALS and FTD with TDP-43 pathology.

Downregulation of TDP-43 Abolishes PNKP Activity in Cultured Neuronal Cells

To further elucidate the mechanism of how PNKP activity might be regulated by functional loss of TDP-43, we performed TDP-43 siRNA (siTDP-43)-mediated knockdown (KD) of TDP-43 in HEK293 cells, which showed a significant KD of TDP-43 without affecting the PNKP protein level, compared to control siRNA (siControl)-treated cells (**Figure 2A**). Consistently, TDP-43 KD revealed a marked decrease in PNKP's 3'-phosphatase activity in siTDP-43 (Ln 4) compared to siControl (Ln 3) cells (**Figure 2B**). These findings indicate that the loss of TDP-43 directly affects PNKP's DNA end-processing functionality, independent of its expression levels, contributing to the observed accumulation of unrepaired DNA breaks in ALS and FTD.

PNKP Overexpression Rescues TDP-43 KD-Associated DNA Damage in Cells

To determine whether PNKP complementation can mitigate TDP-43 depletion-induced DNA damage, we transfected HEK293 cells ectopically expressing FLAG tagged-PNKP with siControl or siTDP-43 and compared the levels of DNA DSB marker γH2AX across the groups, revealing that PNKP overexpression (OE) significantly reduced γH2AX levels in siTDP-43 cells compared to respective control cells (**Figure 3A**). In addition, neutral comet assay under the same conditions as shown in **Figure 3A** demonstrated a marked reduction in DNA DSB in terms of decreased comet tail moment in PNKP-OE + siTDP-43-treated cells compared to only siTDP-43-transfected cells, indicating improved DNA integrity (**Figure 3B**).

To further confirm the effects of PNKP complementation on DNA integrity, long-amplicon quantitative PCR (LA-qPCR) was performed targeting long-range genomic regions of two actively transcribed genes - DNA polymerase beta (POLB) and RNA polymerase II (RNAPII). The analysis demonstrated a significant recovery of DNA integrity as shown by increased PCR band intensity in PNKP-OE cells treated with siTDP-43 compared to siTDP-43 alone treatment. The long amplicon product levels were normalized to a short amplicon product level across the indicated groups (**Figure 3C**).

Our recent studies suggest that the efficient recruitment of the DNA break-sealing complex, XRCC4/ DNA Lig4, is compromised in the absence of functional nuclear TDP-43 (5, 10). The mechanism underlying this disruption, however, remained elusive. Given PNKP's critical role in processing damaged DNA termini at DSB sites to generate ligatable 3'-OH and 5'-P ends, we investigated whether loss of PNKP activity contributes to the impaired recruitment of Lig4 complexes to the DNA DSB sites. Proximity ligation assays (PLA) revealed a significant reduction in Lig4 interactions with γH2AX-marked DSB sites in nuclei of TDP-43 KD cells (**Figure 3D**). This deficiency was effectively rescued in PNKP-OE cells, suggesting that the restoration of PNKP activity enhances the recruitment of DNA Lig4 to genomic DSBs.

TDP-43 Associates with PNKP in the TC-NHEJ Complex and Integrity of Transcribed Genes is Impaired Under Pathological Conditions

Our previous study demonstrates the presence of a pre-formed TC-NHEJ complex involving PNKP and other DSB repair proteins in mammalian brain samples (32, 35). PNKP plays a crucial role in RNA-templated error-free TC-NHEJ repair, thereby protecting the transcribed genome (21, 32, 33). RNA-templated TC-NHEJ is compromised in PNKP-depleted cells. Since our results indicate that either TDP-43 depletion or mislocalization can disrupt PNKP activity, we assessed its association with the TC-NHEJ components in NE from ALS and age-matched control patients' cortical brain samples using PNKP co-immunoprecipitation (co-IP) assay, revealing PNKP's interaction with TDP-43, which was significantly compromised in ALS samples (**Figure 4A**), indicating TDP-43's potential involvement in the TC-NHEJ pathway to facilitate PNKP-mediated DNA DSB repair. We also observed a concomitant decrease in the association of other TC-NHEJ proteins, such as Lig4 and PFKFB3 under pathological conditions (**Figure 4A**). This result was consistent with our previous finding showing disruption of the TC-NHEJ repair pathway in TDP-43 pathology.

Since PNKP is involved in preferential repair of the transcribed genome, we assessed genome damage in actively transcribed versus non-transcribed regions in genomic DNA from cortical tissues of ALS and FTD patients versus age-matched control tissues. Analysis revealed a significant increase in DSB accumulation in transcribed genes (Enolase and NeuroD) compared to

non-transcribed genes (MyH2 and MyH4) in ALS-TDP-43 patient tissues (**Figure 4B**). This preferential accumulation of DNA damage in transcriptionally active regions was consistent with a decrease in PNKP activity and impaired TC-NHEJ repair in TDP-43 pathology.

Reduced PFKFB3 Levels Correlate with Loss of PNKP Activity in ALS and PNKP Activity is Restored by F2,6BP Supplementation

We have demonstrated that F2,6BP, the product of PFKFB3, is a positive co-regulator of PNKP activity *in vivo* (35). We further reported reduced levels of PFKFB3 and F2,6BP in the affected regions of HD and SCA3 patient brain samples - a plausible cause of PNKP inactivation in these pathologies. Therefore, to get further insight into the mechanism of near complete loss of PNKP activity in ALS/FTD, we assessed levels of PFKFB3 and F2,6BP in patients versus age-matched healthy controls. IB analysis revealed a significant decrease in PFKFB3 levels in cortical samples from ALS and FTD patients compared to age-matched controls (**Figure 5A**; *Supplementary* **Figure S1B**). This result was consistent with the observation of reduced PFKFB3 levels associated with the depletion of TDP-43 in HEK293 cells (**Figure 2A**). We further observed that levels of F2,6BP were significantly lower in ALS/FTD patient brain samples compared to age-matched controls (**Figure 5B**), correlating with the reduced levels of PFKFB3 in those samples. These data further suggest a potential link between disrupted glycolytic regulation and impaired DNA repair mechanisms under neurodegenerative conditions. Next, we tested the effect of exogenous F2,6BP supplementation in restoring nuclear PNKP activity in patient samples. Supplementation with F2,6BP significantly restored PNKP activity in the NE of ALS tissues (**Figure 5C**; Lns 7-10 vs. Lns 3-6). We further observed that F2,6BP restored PNKP activity in a dose-dependent manner both in sporadic ALS (**Figure 5D**, Lns 5-6) and Guam-ALS samples **(Figure 5E**, Lns 5-7**)** Notably, we found that only F2,6BP but not F1,6BP or F6P could stimulate PNKP activity, which was in agreement with our previous findings in polyQ diseases (35). These results also highlight that restoring F2,6BP levels can stabilize the PNKP activity, even under stress conditions, thus indicating a metabolic reprogramming-mediated novel regulatory pathway for restoring DNA DSB repair machinery and genome integrity in neurodegenerative diseases.

Characterization of Patient Cell Lines Reveals TDP-43 Pathology-Associated Abrogation of PNKP Activity and Its Subsequent Rescue by F2,6BP Supplementation

To elucidate the impact of ALS and FTD-associated TDP-43 mutations on DNA repair mechanisms, we utilized three ALS and one FTD patient-derived cell lines. Initially, we focused on two ALS-linked TDP-43 mutations G287S and G298S (schematic in **Figure 6A**) and an isogenic CRISPR/Cas9-mediated mutation corrected NPSC line for the G287S mutation (schematic in **Figure 6B**) to elucidate the mechanistic effect of these mutations on DNA DSB repair and PNKP activity. We first examined the subcellular localization of TDP-43 and its phosphorylated form S409/410 (pTDP-43). IF analysis revealed significant cytoplasmic mislocalization of the TDP-43 G287S mutant compared to its isogenic TDP-43^{S287G} variant, which displayed predominantly nuclear TDP-43 (**Figure 6C**). Mander's coefficient of colocalization of total TDP-43 overlapping pTDP-43 and *vice versa* confirmed reduced colocalization of TDP-43 with pTDP-43 in the mutant cells compared to respective control cells, underscoring the nuclear clearance effect of G287S mutation on TDP-43 in ALS.

We next assessed DNA damage in these models by IF-based co-staining of TDP-43 and γH2AX, exhibiting a significant increase in γH2AX foci count in G287S mutant NPCs with higher

signal intensities of cytosolic TDP-43 compared to the isogenic control cells, suggesting a correlation between TDP-43 mislocalization and genomic instability (**Figure 6D**).

Based on these characterizations, we next assessed PFKFB3 levels and 3´-phosphatase activity of PNKP in the G287S mutant vs. its isogenic line to correlate with our earlier results in ALS/FTD patient samples. IB analysis of these cells revealed a significant reduction (~60%) in PFKFB3 protein levels in G287S NPSCs relative to their isogenic controls, while PNKP protein levels remained unaffected (**Figure 6E**). In this line, a marked decrease in PNKP activity was correlated with reduced PFKFB3 levels in these samples, and this loss of activity was restored in a dose-dependent manner by F2,6BP supplementation in vitro (**Figure 6F**). This further demonstrates that reduced PNKP activity is linked to decreased PFKFB3/F2,6BP levels under pathological conditions.

We extended our analysis to TDP-43 G298S mutant NPSCs derived from ALS patients. Similar to the G287S mutant, IF imaging showed cytosolic mislocalization and increased phosphorylation (S409/410) of TDP-43 G298S cells, compared to TDP-43 WT NPSCs, as measured by Mander's coefficient analysis (**Figure 6G**). IB analysis revealed a substantial elevation in γH2AX levels in the G298S mutant, indicating elevated DNA damage, while total H2A.II levels remained comparable between mutant and WT cells (**Figure 6H**). Finally, we assessed PNKP activity in the G298S mutant cells. Similar to our findings with G287S, we observed an ~80% reduction in PNKP activity in G298S NPSCs compared to WT controls, while PNKP activity could be restored by F2,6BP in a dose-dependent manner (**Figure 6I**).

Further investigations extended to an engineered ALS-linked TDP-43 Q331K mutant and its isogenic control (*Supplementary* **Figure S2A**) revealed similar patterns of TDP-43 mislocalization-associated, increased phosphorylation (*Supplementary* **Figure S2B**), reduced PFKFB3 levels (*Supplementary* **Figure S2C**), and decreased PNKP activity (*Supplementary* **Figure SD**), compared to respective controls. In addition, we examined an FTD patient-derived cell line harboring both TDP-43 A282T and a C9ORF72 repeat expansion mutations (*Supplementary* **Figure S2E**) for PNKP activity and the effect of F2,6BP supplementation on FTD iPSCs, which demonstrated a consistent result with other TDP-43 mutant cell lines (*Supplementary* **Figure S2F**), underscoring the therapeutic potential of F2,6BP in restoring DNA repair capacity in TDP-43 pathology.

Altered PNKP Activity and Its Restoration by F2,6BP in ALS-TDP-43 mouse model

Finally, we investigated the impact of TDP-43 pathology on PNKP level and activity in an ALS-TDP-43 mouse model (13). **Figure 7A** shows the schematic of the genetic construct employed to drive murine TDP-43 ΔNLS mutant expression in these mice. We first analyzed the subcellular localization of TDP43 and its phosphorylated form, pTDP-43, in the cortex of both sham and ALS mice by IF (**Figure 7B**). Quantitative analysis using Mander's coefficient demonstrated a significant increase in colocalization of TDP-43 and pTDP-43 in ALS mice brains, emphasizing the pathological redistribution of TDP-43.

We next assessed the levels of PFKFB3 and PNKP in cortical samples from ALS and sham mice. IB analysis revealed a significant reduction in PFKFB3 protein levels in the NE of ALS mice compared to controls, while PNKP levels remained unaltered (**Figure 7C**). We further evaluated PNKP enzymatic function in NE of cortical tissues of ALS and age-matched sham mice (**Figure 7D**), which displayed markedly decreased PNKP activity in ALS mice brains (Lns 6-9) relative to sham controls (Lns 2-5). Importantly, we observed a dose-dependent increase in PNKP activity following F2,6BP supplementation, whereas the glycolytic metabolites F1,6BP and F6P did not

produce similar effects (**Figure 7E**). Overall, these results indicate that TDP-43 pathology in ALS mice leads to significant reductions in PNKP activity. This effect could be correlated with reduced PFKFB3 levels, which was supported by our results that treatment with F2,6BP could effectively rescue PNKP function, suggesting a promising metabolic approach to restoring DNA repair mechanisms in ALS.

Supplementation of F2,6BP restored genome integrity and partially rescued motor phenotype in a *Drosophila* model of ALS

To test the effect of F2,6BP in reversing neurodegenerative phenotype in ALS, we used a fruit fly (*Drosophila melanogaster*) model of ALS where humanized TDP-43 gene with Q331K mutation was expressed under UAS (BDSC# 79590) and crossed with the driver line (BDSC# 64199) to drive motor neuron-specific expression of the mutant TDP-43. The flies were then treated with 1-2 µl of either 50 µM F2,6BP or mock buffer (as control) for 21 days and the motor phenotype was tested by climbing assays. We indeed observed a significant increase in climbing score after supplementation with F2,6BP compared to mock buffer control **(Fig. 8A)**. We further examined the DNA strand break accumulation in *Drosophila CrebB* and *Neurexin* genes by long amplicon qPCR (LA-qPCR). We found an elevated level of DNA damage following Q331K expression compared to the flies used to generate the strains (W^{1118}) **(Fig. 8B, lane 2 vs. lane 1)**. These data further indicate that the mock treatment failed to restore genome integrity. However, significant repair was observed following F2,6BP supplementation **(Fig. 8B, lane 3 vs. lane 2)** and the genome integrity was comparable to that of *w1118* **(Fig. 8C)** that correlated with the rescue of motor phenotype. These findings confirmed the potential of F2,6BP to reverse the ALS neurodegenerative phenotype in a living organism specifically.

Our current study documents the intricate relationship between TDP-43, PNKP, and PFKFB3 in ALS and FTD, as shown schematically in **Figure 9**. By employing patient-derived cells, murine ALS-TDP-43 mouse model, and autopsied ALS and FTD brain tissues, we demonstrate that 3'-phosphatase activity of PNKP is significantly reduced in ALS and FTD, conditions marked by TDP-43 mutations and mislocalization. This decrease in PNKP activity could be attributed to the degradation of PFKFB3 protein under ALS/FTD pathological conditions, and thereby subsequent decrease in the level of its product, F2,6BP, a positive co-factor of PNKP activity. These alterations correlate with the observed DNA damage accumulation in the transcribed genome, an observation consistent with our previous results in PNKP-depleted (21) and PFKFB3-depleted (35) mammalian cell models. Reduction in PNKP activity might lead to the accumulation of "non-ligatable" 3´-Phosphate DNA ends, which may impair the recruitment of XRCC4-Lig4 complex to the DSB sites (as depicted in **Figure 9**), a hallmark of TDP-43 pathology (5, 10, 13). Notably, our results indicate that supplementation with F2,6BP can restore PNKP activity and potentially mitigate genomic instability in neurodegenerative diseases. Overall, our findings suggest that the loss of PNKP activity in TDP-43-associated neurodegeneration is closely tied to disrupted metabolic regulation via PFKFB3. It has now been established that PFKFB3 is stabilized during brain excitation (45). Our results are therefore consistent as they show that PFKFB3's level is low in the nucleus only under ALS/FTD pathogenic conditions but not in post-mitotic healthy neurons. We hypothesize that locally produced F2,6BP is transferred directly to PNKP within the TC-NHEJ complex to potentiate 3´-phosphatase activity of PNKP under normal physiological conditions and this process is severely impaired under pathogenic conditions.

However, the mechanism of PFKFB3 degradation in NE from ALS/FTD patients, mice and patient-derived cells requires further investigation.

While advancements have been made in the treatment of ALS, particularly with the development of therapies targeting specific genetic mutations, FTD remains largely without effective disease-modifying treatments. Riluzole was the first drug approved for ALS therapy. It has been shown to extend patient survival by a few months, however, it did not show any benefit for patients with advanced ALS (46, 47). Another potent antioxidant Edaravone can also halt the disease progression only if given at the early stage of the disease (48, 49). Notably, the landscape of clinical trials targeting TDP-43 in ALS is dynamic, with a variety of therapeutic approaches under investigation (50-52). These efforts reflect a growing recognition of the need to address TDP-43 pathology, which is central to many ALS cases. Continued advancements in this area hold promise for developing effective treatments for ALS patients.

Finally, our study not only elucidates the molecular underpinnings of TDP-43-associated genomic instability but also suggests that targeting metabolic pathways could be a viable therapeutic strategy. By restoring PNKP function through F2,6BP supplementation, we provide a novel approach to counteract the DNA repair deficiencies observed in TDP-43-related neurodegeneration via modulating the glycolytic pathway, offering a new direction for therapeutic development aimed at enhancing the genome maintenance machinery in neurodegenerative conditions.

Supplementary Information

The online version contains supplementary materials, which include supplementary **Figs. S1-2** and **Tables S1-2**.

Acknowledgments

We thank Prof. Ian Robey at the Department of Veterans Affairs Biorepository and Prof. Ralph Garruto at Binghamton Brain Bank for providing the postmortem brain tissue specimens from ALS, Guam-ALS, and FTD patients.

Funding

This research is supported by the National Institute of Neurological Disorders and Stroke of the National Institutes of Health (NIH-NINDS) funds under award numbers RF1NS112719 (M.L.H), R03AG064266 (M.L.H), R01 NS073976 (T. H), R56NS073976 (T. H.), AARG-17-533363. (B.K.), R21AG059223 (B.K.), R01AG063945 (B.K.), R01AI163327 (G.G.) and R21 AG078635 (G.G).

Author contributions

M.L.H. and T.H. conceived and designed the project and edited the final manuscript. A.C. and J.M. performed most of the experiments and wrote the manuscript, with crucial assistance from V.H.M.R., M.K., S.M.M, S.G., S.G.S., V.V., M.M. B.K. and G.G. All authors participated in data analyses and interpretation.

Data availability

All relevant data generated and analyzed in this study are available in this manuscript, online supplementary information or upon reasonable request.

Declarations

Conflict of interest

The authors declare no conflicts of interest.

Ethics Approval

The animal study protocol was approved by the Houston Methodist's Institutional Animal Care and Use Committee under the approval number ISO00006797.

References

1. Neumann M. et al. Ubiquitinated TDP-43 in frontotemporal lobar degeneration and amyotrophic lateral sclerosis. *Science* **314**(5796), 130-133 (2006).
2. Arai T. et al. TDP-43 is a component of ubiquitin-positive tau-negative inclusions in frontotemporal lobar degeneration and amyotrophic lateral sclerosis. *Biochem Biophys Res Commun* **351**(3), 602-611 (2006).
3. Geser F. et al. Pathological TDP-43 in parkinsonism-dementia complex and amyotrophic lateral sclerosis of Guam. *Acta Neuropathol* **115**(1), 133-145 (2008).
4. Feldman E. L. et al. Amyotrophic lateral sclerosis. *Lancet* **400**(10360), 1363-1380 (2022).
5. Mitra J. et al. Motor neuron disease-associated loss of nuclear TDP-43 is linked to DNA double-strand break repair defects. *Proc Natl Acad Sci U S A* **116**(10), 4696-4705 (2019).
6. Highley J. R. et al. Loss of nuclear TDP-43 in amyotrophic lateral sclerosis (ALS) causes altered expression of splicing machinery and widespread dysregulation of RNA splicing in motor neurones. *Neuropathol Appl Neurobiol* **40**(6), 670-685 (2014).
7. Mori F. et al. Colocalization of TDP-43 and stress granules at the early stage of TDP-43 aggregation in amyotrophic lateral sclerosis. *Brain Pathol* **34**(2), e13215 (2024).
8. Fang M. et al. Loss of TDP-43 function contributes to genomic instability in amyotrophic lateral sclerosis. *Front Neurosci* **17**, 1251228 (2023).
9. Konopka A. et al. Impaired NHEJ repair in amyotrophic lateral sclerosis is associated with TDP-43 mutations. *Mol Neurodegener* **15**(1), 51 (2020).
10. Guerrero E. N. et al. Amyotrophic lateral sclerosis-associated TDP-43 mutation Q331K prevents nuclear translocation of XRCC4-DNA ligase 4 complex and is linked to genome damage-mediated neuronal apoptosis. *Hum Mol Genet* **28**(15), 2459-2476 (2019).
11. Giannini M. et al. TDP-43 mutations link Amyotrophic Lateral Sclerosis with R-loop homeostasis and R loop-mediated DNA damage. *PLoS Genet* **16**(12), e1009260 (2020).
12. Hill S. J. et al. Two familial ALS proteins function in prevention/repair of transcription-associated DNA damage. *Proc Natl Acad Sci U S A* **113**(48), E7701-e7709 (2016).
13. Mitra J. et al. Endogenous TDP-43 mislocalization in a novel knock-in mouse model reveals DNA repair impairment, inflammation, and neuronal senescence. *Res Sq*, (2024).
14. Lopez-Gonzalez R. et al. Poly(GR) in C9ORF72-Related ALS/FTD Compromises Mitochondrial Function and Increases Oxidative Stress and DNA Damage in iPSC-Derived Motor Neurons. *Neuron* **92**(2), 383-391 (2016).
15. Kay J., Thadhani E., Samson L., Engelward B. Inflammation-induced DNA damage, mutations and cancer. *DNA Repair (Amst)* **83**, 102673 (2019).
16. Pálmai-Pallag T., Bachrati C. Z. Inflammation-induced DNA damage and damage-induced inflammation: a vicious cycle. *Microbes Infect* **16**(10), 822-832 (2014).

17. Kiraly O., Gong G., Olipitz W., Muthupalani S., Engelward B. P. Inflammation-induced cell proliferation potentiates DNA damage-induced mutations in vivo. *PLoS Genet* **11**(2), e1004901 (2015).
18. Lan L. et al. In situ analysis of repair processes for oxidative DNA damage in mammalian cells. *Proc Natl Acad Sci U S A* **101**(38), 13738-13743 (2004).
19. Jilani A. et al. Molecular cloning of the human gene, PNKP, encoding a polynucleotide kinase 3'-phosphatase and evidence for its role in repair of DNA strand breaks caused by oxidative damage. *J Biol Chem* **274**(34), 24176-24186 (1999).
20. Karimi-Busheri F. et al. Molecular characterization of a human DNA kinase. *J Biol Chem* **274**(34), 24187-24194 (1999).
21. Chakraborty A. et al. Classical non-homologous end-joining pathway utilizes nascent RNA for error-free double-strand break repair of transcribed genes. *Nat Commun* **7**, 13049 (2016).
22. Wiederhold L. et al. AP endonuclease-independent DNA base excision repair in human cells. *Mol Cell* **15**(2), 209-220 (2004).
23. Das A. et al. NEIL2-initiated, APE-independent repair of oxidized bases in DNA: Evidence for a repair complex in human cells. *DNA Repair (Amst)* **5**(12), 1439-1448 (2006).
24. Aceytuno R. D. et al. Structural and functional characterization of the PNKP-XRCC4-LigIV DNA repair complex. *Nucleic Acids Res* **45**(10), 6238-6251 (2017).
25. Shen J. et al. Mutations in PNKP cause microcephaly, seizures and defects in DNA repair. *Nat Genet* **42**(3), 245-249 (2010).
26. Poulton C. et al. Progressive cerebellar atrophy and polyneuropathy: expanding the spectrum of PNKP mutations. *Neurogenetics* **14**(1), 43-51 (2013).
27. Bras J. et al. Mutations in PNKP cause recessive ataxia with oculomotor apraxia type 4. *Am J Hum Genet* **96**(3), 474-479 (2015).
28. Shimada M., Dumitrache L. C., Russell H. R., McKinnon P. J. Polynucleotide kinase-phosphatase enables neurogenesis via multiple DNA repair pathways to maintain genome stability. *Embo j* **34**(19), 2465-2480 (2015).
29. Islam A. et al. Functional analysis of a conserved site mutation in the DNA end processing enzyme PNKP leading to ataxia with oculomotor apraxia type 4 in humans. *J Biol Chem* **299**(5), 104714 (2023).
30. Dumitrache L. C., McKinnon P. J. Polynucleotide kinase-phosphatase (PNKP) mutations and neurologic disease. *Mech Ageing Dev* **161**(Pt A), 121-129 (2017).
31. Gao R. et al. Mutant huntingtin impairs PNKP and ATXN3, disrupting DNA repair and transcription. *Elife* **8**, (2019).
32. Chakraborty A. et al. Deficiency in classical nonhomologous end-joining-mediated repair of transcribed genes is linked to SCA3 pathogenesis. *Proc Natl Acad Sci U S A* **117**(14), 8154-8165 (2020).
33. Chakraborty A. et al. Human DNA polymerase η promotes RNA-templated error-free repair of DNA double-strand breaks. *J Biol Chem* **299**(3), 102991 (2023).
34. Welsh J. A. et al. Minimal information for studies of extracellular vesicles (MISEV2023): From basic to advanced approaches. *J Extracell Vesicles* **13**(2), e12404 (2024).
35. Chakraborty A. et al. Fructose-2,6-bisphosphate restores DNA repair activity of PNKP and ameliorates neurodegenerative symptoms in Huntington's disease. *Proc Natl Acad Sci U S A* **121**(39), e2406308121 (2024).

36. Moretton A., Loizou J. I. Interplay between Cellular Metabolism and the DNA Damage Response in Cancer. *Cancers (Basel)* **12**(8), (2020).
37. Ros S., Schulze A. Balancing glycolytic flux: the role of 6-phosphofructo-2-kinase/fructose 2,6-bisphosphatases in cancer metabolism. *Cancer Metab* **1**(1), 8 (2013).
38. Yalcin A. et al. Nuclear targeting of 6-phosphofructo-2-kinase (PFKFB3) increases proliferation via cyclin-dependent kinases. *J Biol Chem* **284**(36), 24223-24232 (2009).
39. Gustafsson N. M. S. et al. Targeting PFKFB3 radiosensitizes cancer cells and suppresses homologous recombination. *Nat Commun* **9**(1), 3872 (2018).
40. Chakraborty A. et al. F2,6BP restores mitochondrial genome integrity in Huntington's Disease. *bioRxiv*, 2024.2011.2004.621834 (2024).
41. Fazal R. et al. HDAC6 inhibition restores TDP-43 pathology and axonal transport defects in human motor neurons with TARDBP mutations. *Embo j* **40**(7), e106177 (2021).
42. Smith A. S. T. et al. Human Induced Pluripotent Stem Cell-Derived TDP-43 Mutant Neurons Exhibit Consistent Functional Phenotypes Across Multiple Gene Edited Lines Despite Transcriptomic and Splicing Discrepancies. *Front Cell Dev Biol* **9**, 728707 (2021).
43. Kodavati M. et al. FUS unveiled in mitochondrial DNA repair and targeted ligase-1 expression rescues repair-defects in FUS-linked motor neuron disease. *Nat Commun* **15**(1), 2156 (2024).
44. Wang H. et al. Mutant FUS causes DNA ligation defects to inhibit oxidative damage repair in Amyotrophic Lateral Sclerosis. *Nat Commun* **9**(1), 3683 (2018).
45. Díaz-García C. M. et al. Neuronal Stimulation Triggers Neuronal Glycolysis and Not Lactate Uptake. *Cell Metab* **26**(2), 361-374.e364 (2017).
46. Saitoh Y., Takahashi Y. Riluzole for the treatment of amyotrophic lateral sclerosis. *Neurodegener Dis Manag* **10**(6), 343-355 (2020).
47. Petrov D., Mansfield C., Moussy A., Hermine O. ALS Clinical Trials Review: 20 Years of Failure. Are We Any Closer to Registering a New Treatment? *Front Aging Neurosci* **9**, 68 (2017).
48. Cho H., Shukla S. Role of Edaravone as a Treatment Option for Patients with Amyotrophic Lateral Sclerosis. *Pharmaceuticals (Basel)* **14**(1), (2020).
49. Brooks B. R. et al. Intravenous edaravone treatment in ALS and survival: An exploratory, retrospective, administrative claims analysis. *EClinicalMedicine* **52**, 101590 (2022).
50. Khamaysa M., Pradat P. F. Status of ALS Treatment, Insights into Therapeutic Challenges and Dilemmas. *J Pers Med* **12**(10), (2022).
51. Afroz T. et al. Immunotherapy targeting the C-terminal domain of TDP-43 decreases neuropathology and confers neuroprotection in mouse models of ALS/FTD. *Neurobiol Dis* **179**, 106050 (2023).
52. Fang M. Y. et al. Small-Molecule Modulation of TDP-43 Recruitment to Stress Granules Prevents Persistent TDP-43 Accumulation in ALS/FTD. *Neuron* **103**(5), 802-819.e811 (2019).

Figure 1

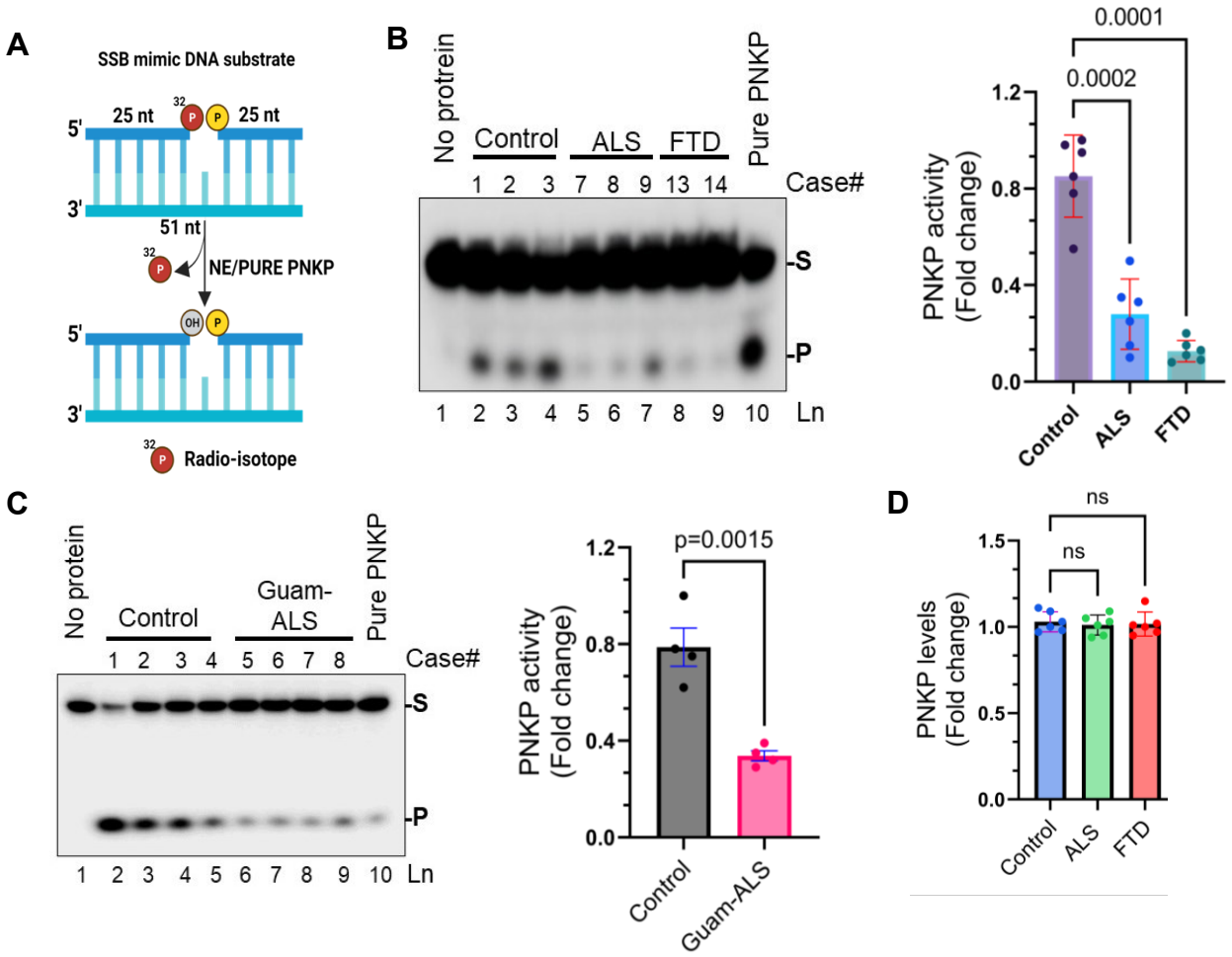
A
SSB mimic DNA substrate
25 nt
25 nt
5'
3'
51 nt
NE/PURE PNKP
5'
3'
Radio-isotope
B
No protrein
Control
ALS
FTD
Pure PNKP
Case#
1 2 3 7 8 9 13 14
S
P
1 2 3 4 5 6 7 8 9 10 Ln
PNKP activity (Fold change)
0.0001
0.0002
Control
ALS
FTD
C
No protein
Control
Guam-ALS
Pure PNKP
Case#
1 2 3 4 5 6 7 8
S
P
1 2 3 4 5 6 7 8 9 10 Ln
PNKP activity (Fold change)
p=0.0015
Control
Guam-ALS
D
PNKP levels (Fold change)
ns
ns
Control
ALS
FTD

Figure 2

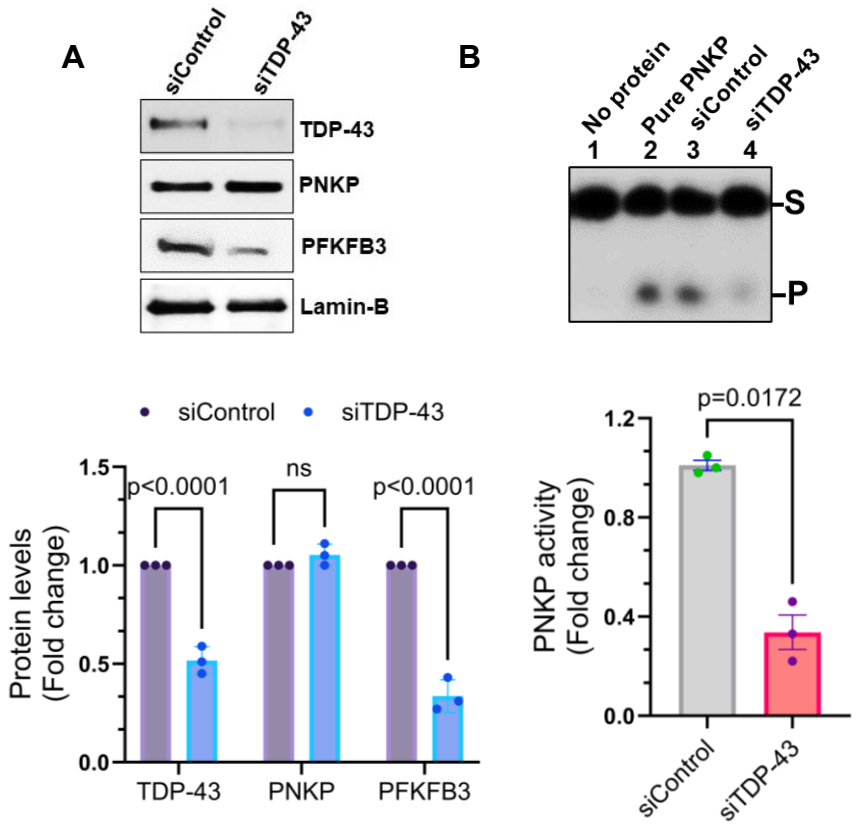
A
siControl
siTDP-43
TDP-43
PNKP
PFKFB3
Lamin-B
B
No protein
Pure PNKP
siControl
siTDP-43
1
2
3
4
S
P
siControl
siTDP-43
Protein levels
(Fold change)
1.5
1.0
0.5
0.0
p<0.0001
ns
p<0.0001
TDP-43
PNKP
PFKFB3
p=0.0172
PNKP activity
(Fold change)
1.2
0.8
0.4
0.0
siControl
siTDP-43

Figure 3

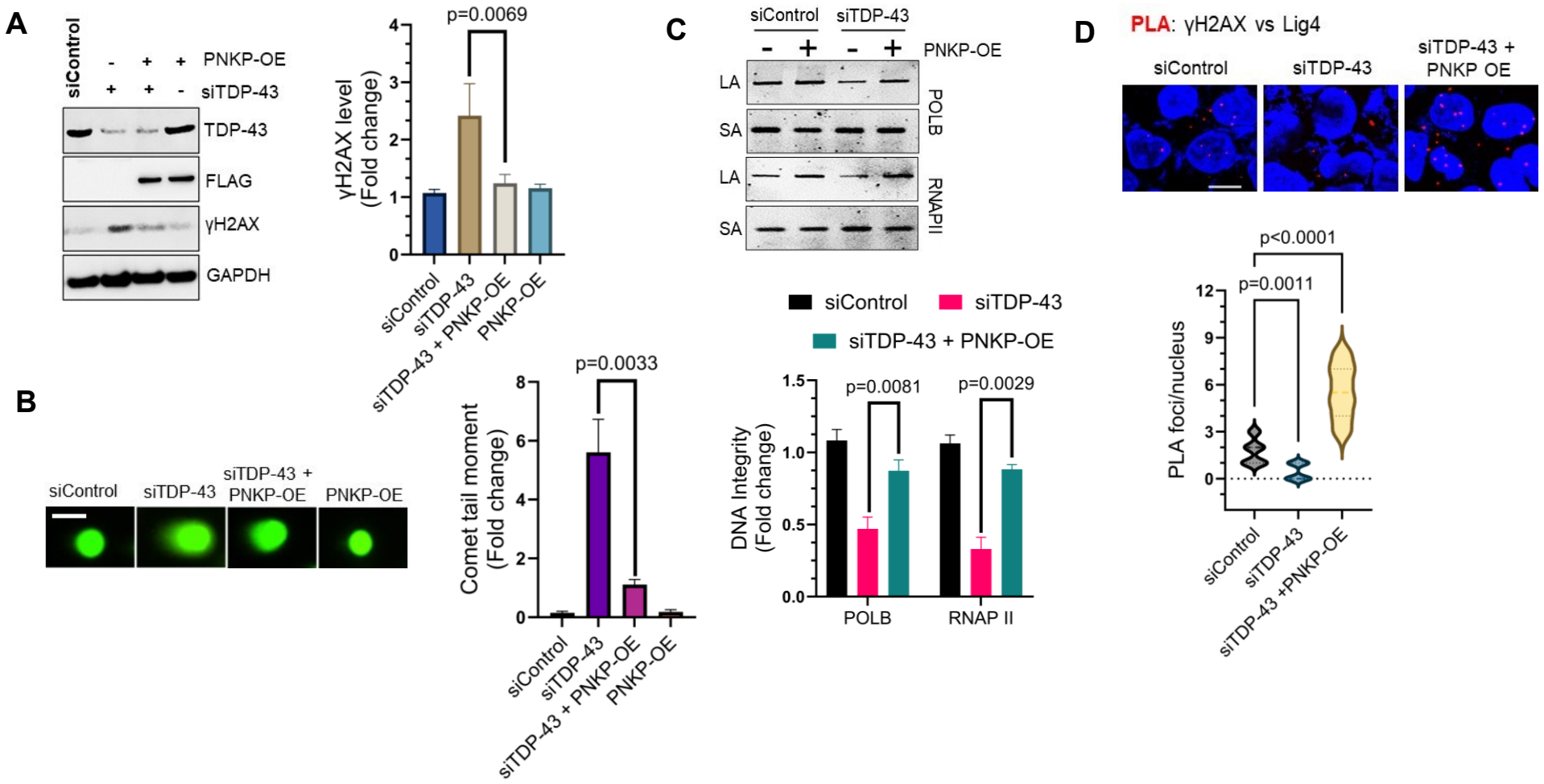
A
siControl
PNKP-OE
siTDP-43
TDP-43
FLAG
γH2AX
GAPDH
p=0.0069
γH2AX level (Fold change)
siControl
siTDP-43
siTDP-43 + PNKP-OE
PNKP-OE
B
siControl
siTDP-43
siTDP-43 + PNKP-OE
PNKP-OE
p=0.0033
Comet tail moment (Fold change)
C
siControl
siTDP-43
PNKP-OE
LA
SA
POLB
RNAPII
siTDP-43 + PNKP-OE
p=0.0081
p=0.0029
DNA Integrity (Fold change)
POLB
RNAP II
D
PLA: γH2AX vs Lig4
siTDP-43 + PNKP OE
p<0.0001
p=0.0011
PLA foci/nucleus

Figure 4

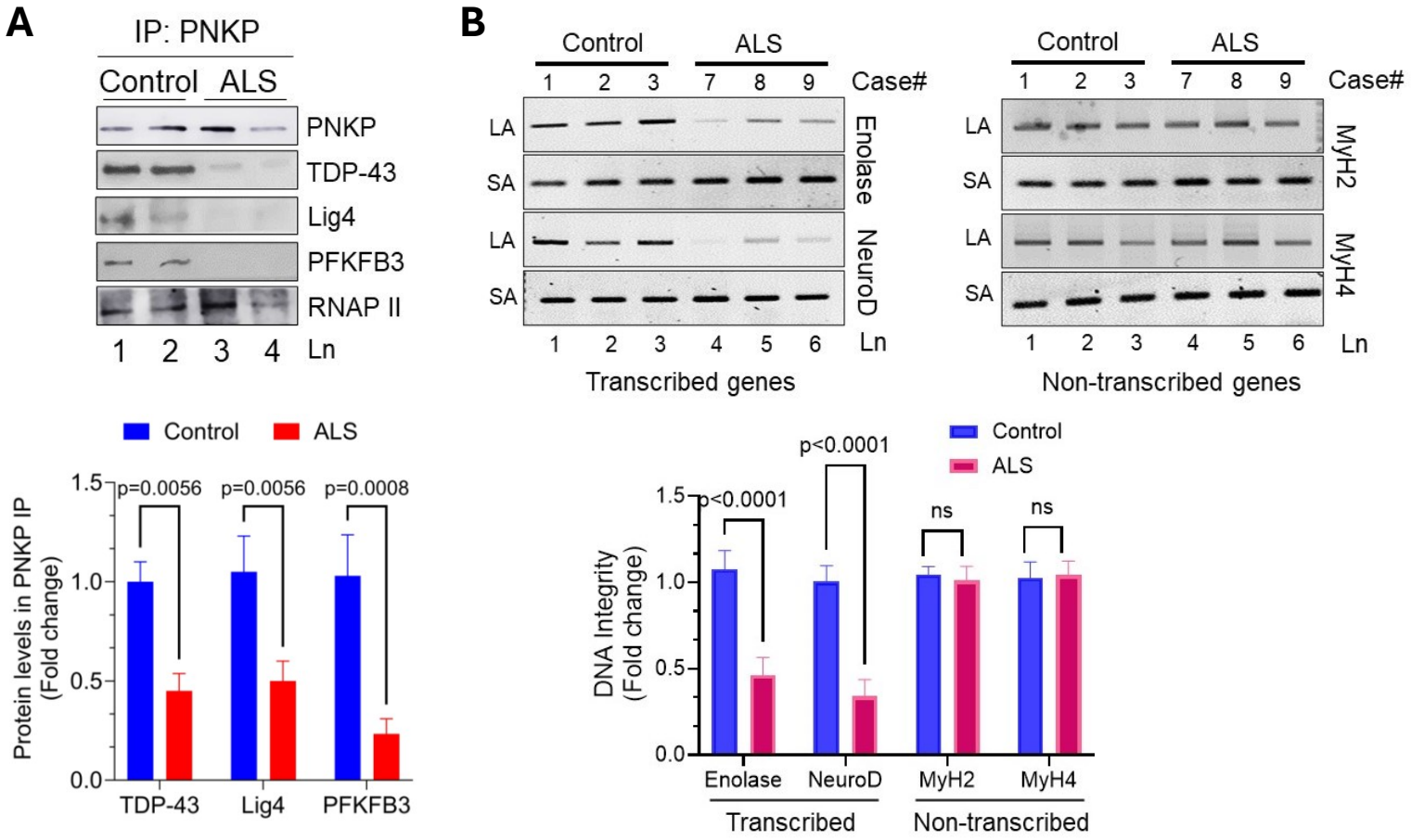
A
IP: PNKP
Control
ALS
PNKP
TDP-43
Lig4
PFKFB3
RNAP II
1 2 3 4 Ln
Control
ALS
Protein levels in PNKP IP (Fold change)
1.5
1.0
0.5
0.0
p=0.0056
p=0.0056
p=0.0008
TDP-43
Lig4
PFKFB3
B
Control
ALS
1 2 3 7 8 9 Case#
LA
SA
LA
SA
Enolase
NeuroD
1 2 3 4 5 6 Ln
Transcribed genes
Control
ALS
1 2 3 7 8 9 Case#
LA
SA
LA
SA
MyH2
MyH4
1 2 3 4 5 6 Ln
Non-transcribed genes
Control
ALS
DNA Integrity (Fold change)
1.5
1.0
0.5
0.0
p<0.0001
p<0.0001
ns
ns
Enolase
NeuroD
MyH2
MyH4
Transcribed
Non-transcribed

Figure 5

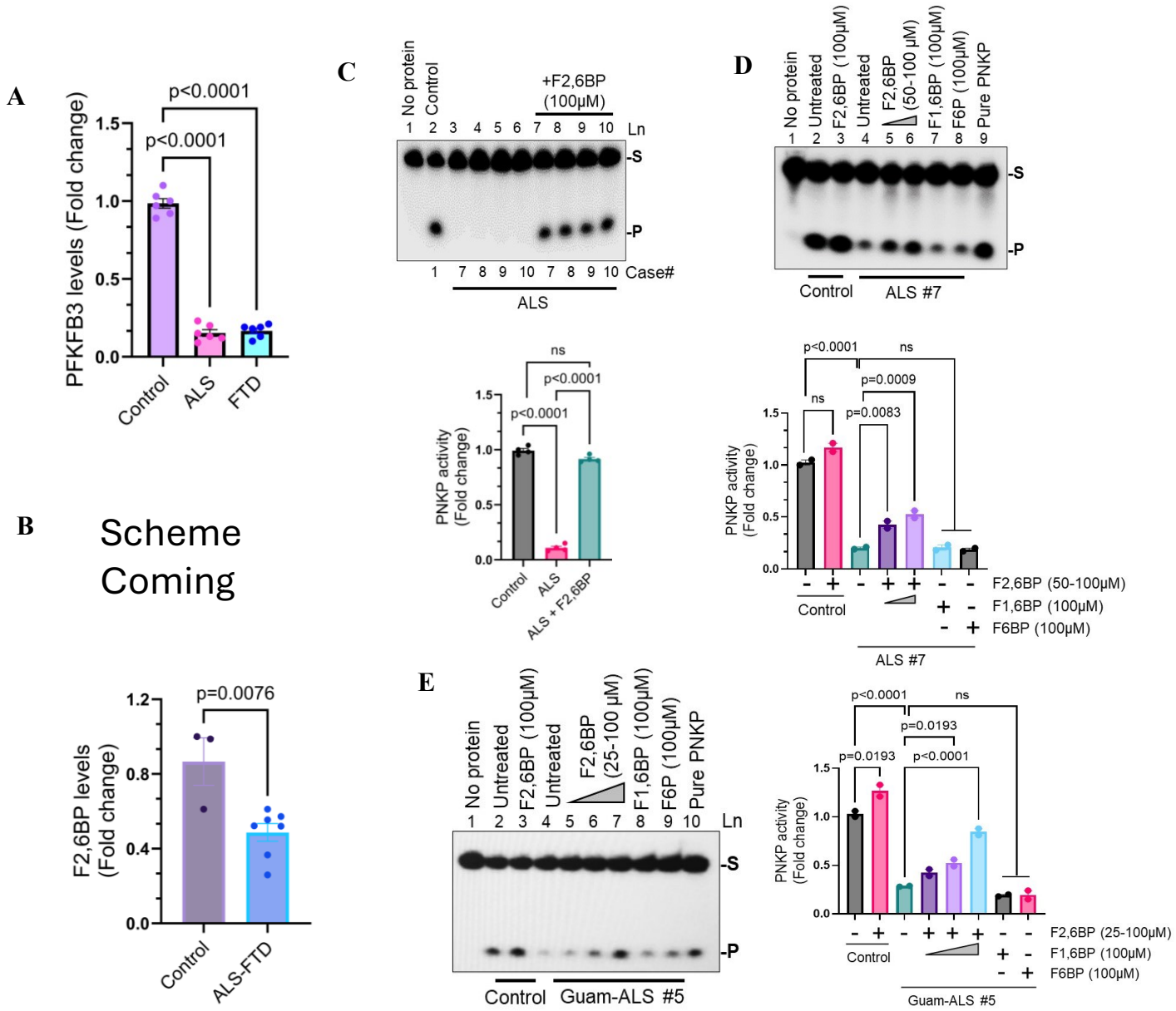
A
PFKFB3 levels (Fold change)
p<0.0001
p<0.0001
Control
ALS
FTD
B
Scheme Coming
F2,6BP levels (Fold change)
p=0.0076
Control
ALS-FTD
C
No protein
Control
+F2,6BP (100μM)
Ln
-S
-P
Case#
ALS
PNKP activity (Fold change)
ns
p<0.0001
p<0.0001
Control
ALS
ALS + F2,6BP
D
No protein
Untreated
F2,6BP (100μM)
Untreated
F2,6BP (50-100 μM)
F1,6BP (100μM)
F6P (100μM)
Pure PNKP
Control
ALS #7
p<0.0001
ns
p=0.0009
ns
p=0.0083
F2,6BP (50-100μM)
F1,6BP (100μM)
F6BP (100μM)
E
No protein
Untreated
F2,6BP (100μM)
Untreated
F2,6BP (25-100 μM)
F1,6BP (100μM)
F6P (100μM)
Pure PNKP
Control
Guam-ALS #5
p<0.0001
ns
p=0.0193
p=0.0193
p<0.0001
F2,6BP (25-100μM)
F1,6BP (100μM)
F6BP (100μM)

Figure 6

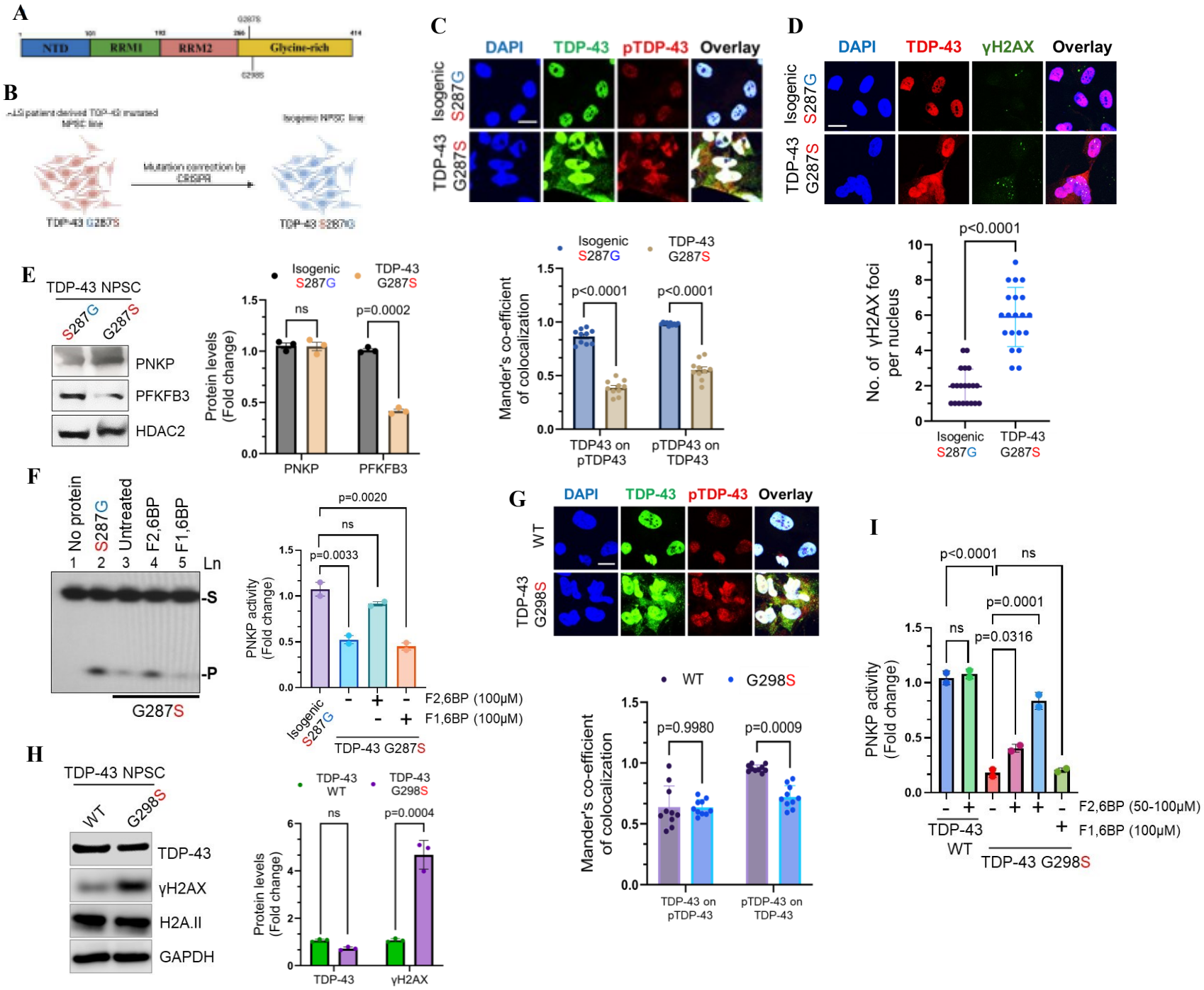
A
NTD
RRM1
RRM2
Glycine-rich
B
Mutation correction by CRISPR
TDP-43 G287S
TDP-43 S287G
C
DAPI
TDP-43
pTDP-43
Overlay
Isogenic S287G
TDP-43 G287S
D
DAPI
TDP-43
γH2AX
Overlay
Isogenic S287G
TDP-43 G287S
E
TDP-43 NPSC
S287G
G287S
PNKP
PFKFB3
HDAC2
Isogenic S287G
TDP-43 G287S
Protein levels (Fold change)
ns
p=0.0002
PNKP
PFKFB3
Mander's co-efficient of colocalization
p<0.0001
p<0.0001
TDP43 on pTDP43
pTDP43 on TDP43
No. of γH2AX foci per nucleus
p<0.0001
Isogenic S287G
TDP-43 G287S
F
No protein
S287G
Untreated
F2,6BP
F1,6BP
Ln
-S
-P
G287S
PNKP activity (Fold change)
p=0.0020
ns
p=0.0033
F2,6BP (100μM)
F1,6BP (100μM)
Isogenic S287G
TDP-43 G287S
G
DAPI
TDP-43
pTDP-43
Overlay
WT
TDP-43 G298S
WT
G298S
Mander's co-efficient of colocalization
p=0.9980
p=0.0009
TDP-43 on pTDP-43
pTDP-43 on TDP-43
H
TDP-43 NPSC
WT
G298S
TDP-43
γH2AX
H2A.II
GAPDH
TDP-43 WT
TDP-43 G298S
ns
p=0.0004
Protein levels (Fold change)
TDP-43
γH2AX
I
p<0.0001
ns
p=0.0001
ns
p=0.0316
PNKP activity (Fold change)
F2,6BP (50-100μM)
F1,6BP (100μM)
TDP-43 WT
TDP-43 G298S

Figure 7

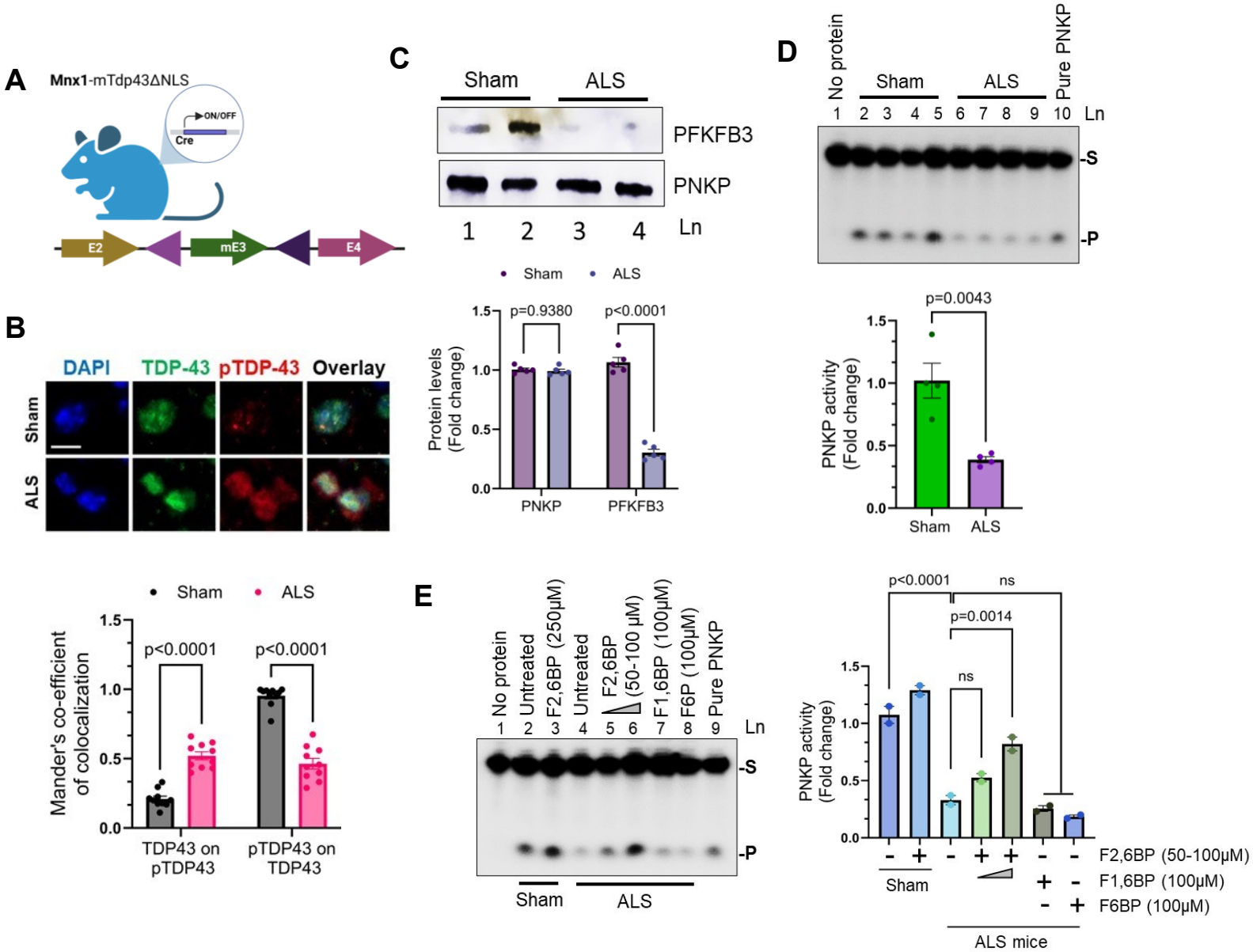
A
Mnx1-mTdp43ΔNLS
ON/OFF
Cre
E2
mE3
E4
B
DAPI
TDP-43
pTDP-43
Overlay
Sham
ALS
Sham
ALS
Mander's co-efficient of colocalization
p<0.0001
p<0.0001
TDP43 on pTDP43
pTDP43 on TDP43
C
Sham
ALS
PFKFB3
PNKP
1 2 3 4 Ln
Sham
ALS
Protein levels (Fold change)
p=0.9380
p<0.0001
PNKP
PFKFB3
D
No protein
Sham
ALS
Pure PNKP
1 2 3 4 5 6 7 8 9 10 Ln
-S
-P
p=0.0043
PNKP activity (Fold change)
Sham
ALS
E
No protein
Untreated
F2,6BP (250μM)
Untreated
F2,6BP (50-100 μM)
F1,6BP (100μM)
F6P (100μM)
Pure PNKP
1 2 3 4 5 6 7 8 9 Ln
-S
-P
Sham
ALS
p<0.0001
ns
p=0.0014
ns
PNKP activity (Fold change)
F2,6BP (50-100μM)
F1,6BP (100μM)
F6BP (100μM)
Sham
ALS mice

Figure 8

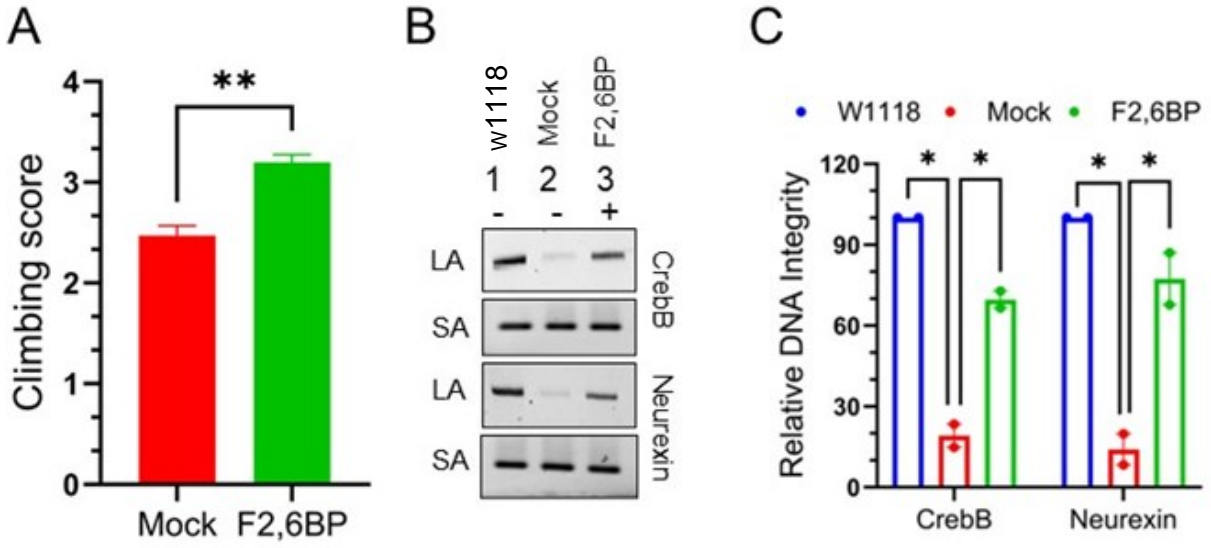
A
Climbing score
4
3
2
1
0
**
Mock
F2,6BP
B
w1118
Mock
F2,6BP
1
2
3
-
-
+
LA
SA
LA
SA
CrebB
Neurexin
C
W1118
Mock
F2,6BP
Relative DNA Integrity
120
90
60
30
0
*
*
*
*
CrebB
Neurexin

Figure 9

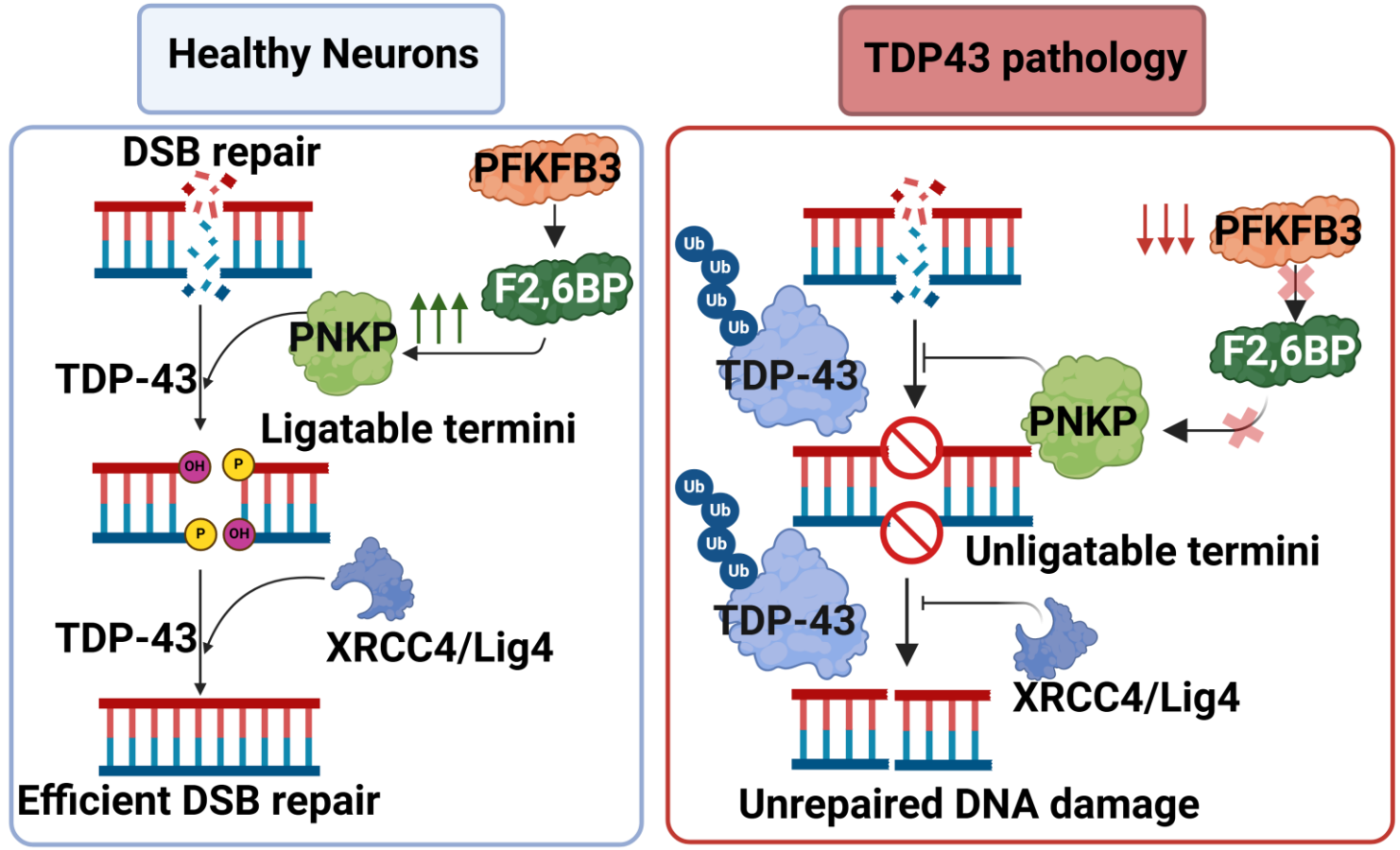
Healthy Neurons
DSB repair
PFKFB3
F2,6BP
PNKP
TDP-43
Ligatable termini
OH
P
P
OH
TDP-43
XRCC4/Lig4
Efficient DSB repair
TDP43 pathology
Ub
Ub
Ub
Ub
TDP-43
PFKFB3
F2,6BP
PNKP
Unligatable termini
Ub
Ub
Ub
Ub
TDP-43
XRCC4/Lig4
Unrepaired DNA damage